nature structural & molecular biology

Structural basis for aminoglycoside inhibition of bacterial ribosome recycling

Maria A Borovinskaya[1,8], Raj D Pai[2,8], Wen Zhang[3,8], Barbara S Schuwirth[3,7], James M Holton[1,4], Go Hirokawa[5,7], Hideko Kaji[6], Akira Kaji[5] & Jamie H Doudna Cate[1–3]

Aminoglycosides are widely used antibiotics that cause messenger RNA decoding errors, block mRNA and transfer RNA translocation, and inhibit ribosome recycling. Ribosome recycling follows the termination of protein synthesis and is aided by ribosome recycling factor (RRF) in bacteria. The molecular mechanism by which aminoglycosides inhibit ribosome recycling is unknown. Here we show in X-ray crystal structures of the *Escherichia coli* 70S ribosome that RRF binding causes RNA helix H69 of the large ribosomal subunit, which is crucial for subunit association, to swing away from the subunit interface. Aminoglycosides bind to H69 and completely restore the contacts between ribosomal subunits that are disrupted by RRF. These results provide a structural explanation for aminoglycoside inhibition of ribosome recycling.

Aminoglycosides are one of the most clinically important classes of antibiotics that inhibit bacterial protein synthesis by targeting the ribosome[1]. They are also excellent templates for antibiotic design because of their high binding affinity and properties that allow for broad-spectrum antibacterial activity[2]. The structurally related aminoglycosides neomycin, paromomycin and gentamicin possess 4,5-substituted and 4,6-substituted 2-deoxystreptamine cores (**Fig. 1a**). These compounds exert multiple effects on protein synthesis: they cause mRNA miscoding[3,4], inhibit mRNA and tRNA translocation[5,6] and inhibit ribosome recycling[7]. Understanding the mechanisms by which aminoglycosides inhibit ribosome function will aid in creating new clinically useful drugs that selectively target the bacterial ribosome.

Ribosome recycling completes each cycle of protein synthesis. It is also involved in reactivation of idled ribosomes in bacteria recovering from stress or slow-growth conditions[8,9]. In bacteria, ribosome recycling factor (RRF) helps to separate the 70S ribosome into its small (30S) and large (50S) ribosomal subunits, thereby recycling the subunits for use in subsequent rounds of translation. RRF works in concert with the GTPase elongation factor G (EF-G) to drive ribosomal subunit dissociation[10–13]. RRF also helps to dissociate vacant 70S ribosomes into subunits *in vitro*[14], and does the same for idled 70S ribosomes *in vivo*[9]. RRF exists in bacteria[13], mitochondria[15] and chloroplasts[16], and absence of the protein in bacteria is lethal[9,17]. At present, it is not known how aminoglycosides interfere with the mechanism of ribosome recycling.

Neomycin and gentamicin have been shown biochemically to bind to the ribosome at two sites, one in each ribosomal subunit[6,18]. The binding site for this class of antibiotics in RNA helix 44 of the small ribosomal subunit (h44) has been well characterized at the genetic, biochemical and structural levels[1,19,20]. However, no data on the aminoglycoside-binding site in the large ribosomal subunit has been available so far. To shed light on the location and potential functional role of this site, we determined structures of the *E. coli* 70S ribosome in complexes with the aminoglycosides neomycin and gentamicin[6], with RRF, and with RRF plus gentamicin or paromomycin[7].

RESULTS

Aminoglycoside binding to the 70S ribosome

Difference electron density maps comparing antibiotic-soaked ribosomes with apo–70S ribosomes[21] revealed two primary binding sites in the ribosome for gentamicin and neomycin (**Fig. 1** and **Fig. 2a**,**b**). In addition to the well-known binding site located in the mRNA-decoding center in h44 of the small ribosomal subunit[19,20,22], the antibiotics also bind to RNA helix 69 of the large ribosomal subunit (H69; **Figs. 1** and **2**). H69 forms several intersubunit bridges with the 30S subunit[21,23] and makes direct contacts with aminoacyl- and peptidyl-tRNAs (A- and P-site tRNAs)[20,23]. The closing loop of H69 directly contacts the small subunit at the mRNA-decoding center, while its stem forms part of the P site (**Fig. 1c**). The aminoglycoside-binding site is in the major groove of H69 at the base of its stem, which would contact P-site tRNA (**Fig. 1c**).

[1]Physical Biosciences Division, Lawrence Berkeley National Laboratory, Berkeley, California 94720, USA. [2]Department of Molecular and Cell Biology and [3]Department of Chemistry, University of California, Berkeley, California 94720, USA. [4]Department of Biochemistry and Biophysics, University of California, San Francisco, California 94158, USA. [5]Department of Microbiology, University of Pennsylvania School of Medicine, Philadelphia, Pennsylvania 19104, USA. [6]Department of Biochemistry and Molecular Biology, Thomas Jefferson University, Philadelphia, Pennsylvania 19107, USA. [7]Present addresses: Cancer Research UK London Research Institute, Clare Hall Laboratories, South Mimms, Hertfordshire EN6 3LD, UK (B.S.S.) and National Cardiovascular Center Research Institute, Osaka, Japan (G.H.). [8]These authors contributed equally to this work. Correspondence should be addressed to J.H.D.C. (jcate@lbl.gov).

Received 12 April; accepted 11 June; published online 29 July 2007; doi:10.1038/nsmb1271

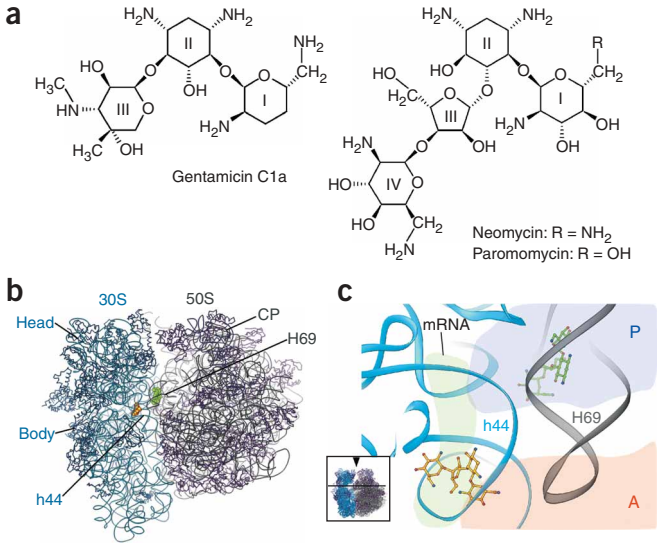

Figure 1 Interactions of aminoglycosides with h44 and H69 of the ribosome. (**a**) Chemical structures of neomycin, paromomycin and gentamicin. (**b**) Global view of the ribosome and the two binding sites for aminoglycosides. Gold and green, aminoglycosides bound to the 30S and 50S subunits, respectively; light blue, 16S rRNA; gray, 23S rRNA; purple, 5S rRNA; dark blue and magenta, proteins of small and large subunits, respectively; CP, central protuberance. (**c**) Close-up view of the two binding sites in h44 and H69, shown with neomycin as an example. Neomycin molecules bound to h44 and H69 are in gold and green, respectively. Green, orange and blue shadows outline positions that would be occupied by mRNA, A-site tRNA and P-site tRNA, respectively. The mRNA and tRNAs are above the plane of the image. Inset shows direction of view.

Most of the ribosomal RNA residues in H69 that form the aminoglycoside-binding site are highly or universally conserved among bacteria[24] (**Fig. 2c**). Rings I and II of neomycin and gentamicin make similar contacts to nucleotides C1920–C1925 and G1906 in H69, and probably provide the primary binding determinants (**Fig. 2a**,**b**). Ring I of neomycin also contacts G1929 in H69, while ring IV of neomycin extends toward G1517 in the 30S subunit (**Fig. 2a**).

Aminoglycoside effects on RRF-ribosome interactions

Given the location of the aminoglycoside-binding site in H69, at the heart of the ribosome-recycling and translocation processes[11,25–28], this site may be important in aminoglycoside inhibition of ribosome recycling[7]. To test this model, we determined structures of *Thermus thermophilus* RRF bound to the 70S ribosome[29]. The crystals used in the structure determination contain two ribosomes per asymmetric unit, termed I and II, that adopt different conformations and have different degrees of subunit packing[21] (**Supplementary Data** online). In structures of the 70S ribosome in complex with RRF, RRF binds to the large subunits[11,25,27,30] of both ribosomes in the crystals and induces H69 to swing away from the subunit interface in ribosome I (**Fig. 3**, **Supplementary Data** and **Supplementary Fig. 1** online). Although RRF binds to ribosome II, it is able to dissociate H69 from the interface in only a small percentage of these ribosomes (**Supplementary Data**), in contrast to its effect on ribosome I in these crystals (**Fig. 3** and **Supplementary Fig. 1**) and its previously reported effect seen in cryo-EM reconstructions[27]. The conformational change in H69 breaks key bridges between the ribosomal subunits that are important for subunit association[31]. The structural rearrangement induced by RRF involves an overwinding of the helical pitch of H69 and leads to a high degree of dynamics in the helix (**Fig. 3b**). The greater disorder near the tip of H69 in the crystals is consistent with changes seen in low-resolution cryo-EM reconstructions of the ribosome with RRF bound[27], indicating that the conformational change in ribosome I in the crystals accurately reflects processes taking place in solution (**Supplementary Data** and **Supplementary Fig. 1**).

Notably, in structures of the ribosome in complex with RRF and either gentamicin or paromomycin, the effect of RRF on H69 dynamics is completely suppressed (**Fig. 4** and **Supplementary Fig. 2** online), consistent with aminoglycoside inhibition of ribosome recycling[7]. The bridges between the two ribosomal subunits are re-established in conformations nearly identical to those seen in the presence of the antibiotics alone, in the absence of RRF (**Figs. 1**, **2** and **4**, and **Supplementary Fig. 2**)[20]. In addition to binding to H69, the aminoglycosides also bind to the small ribosomal subunit at the mRNA-decoding center, as has been observed in other structures[19,20]. However, the H69 binding site is probably important in inhibiting the effects of RRF, for steric reasons. In the structures, the major groove of H69 is wide enough to bind the aminoglycosides only in the conformation of H69 that forms bridges with the small subunit, and not in the RRF-induced conformation, in which H69 swings away from the subunit interface (**Fig. 4c**). Furthermore, ribosome structures determined with low and high concentrations of aminoglycosides

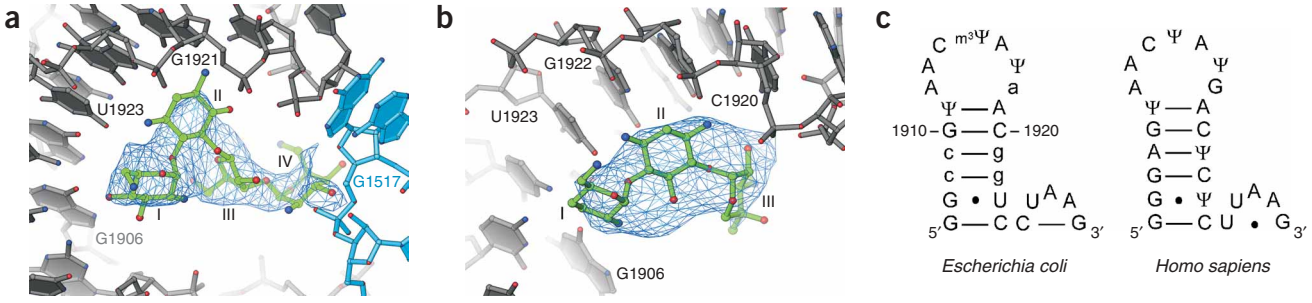

Figure 2 Interactions of aminoglycosides with H69 of the ribosome. (**a**,**b**) $F_o - F_o$ difference Fourier electron density maps of neomycin (**a**) and gentamicin (**b**) binding sites in H69, colored as in **Figure 1b**. For clarity, positive electron density is shown only in the vicinity of the antibiotics. Roman numerals denote rings in the aminoglycosides, as in **Figure 1a**. (**c**) Secondary structure of H69 within 23S rRNA in the 50S subunit, and its sequence conservation in bacteria (left) and eukaryotes (right)[24]. Capital letters denote positions with more than 95% conservation within each respective kingdom; lowercase letters denote positions with 88%–95% conservation within each kingdom. Nucleotides 1906–1929 of 23S rRNA are shown for *E. coli*; the corresponding nucleotides (3722–3745) of 28S rRNA are shown for *H. sapiens*.

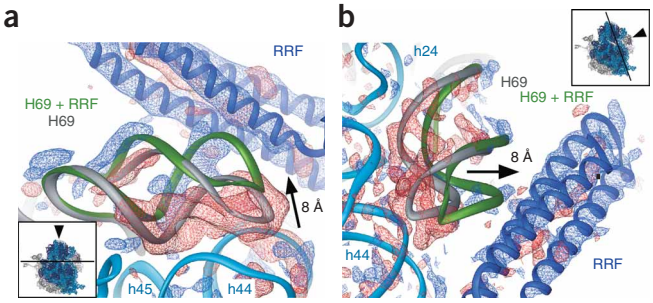

Figure 3 Structural effects of RRF binding to ribosome I. (**a**) $F_o - F_o$ difference electron density map, truncated at 6-Å resolution, comparing 70S ribosome crystals in complex with RRF to ribosomes in complex with neomycin. In the absence of RRF, the overall position of H69 at the interface in apo–70S ribosomes is essentially identical to that in neomycin-bound ribosomes (**Supplementary Methods**). Only domain I of RRF is visible; domain II is located to the right of the view shown. Blue, positive difference density; red, negative difference density; arrow, direction of the conformational change in H69 upon RRF binding. (**b**) $F_o - F_o$ difference electron density as in **a**, but at 3.5-Å resolution. Insets in **a** and **b** show angles of view.

reveal that binding of an aminoglycoside to H69, when h44 is already saturated with the antibiotic, suppresses the RRF-induced conformational change in H69 (**Fig. 4d**, **Supplementary Data** and **Supplementary Fig. 3** online).

DISCUSSION

In bacteria, RRF functions with EF-G to separate the 70S ribosome into its 30S and 50S ribosomal subunits, thereby recycling the subunits for use in subsequent rounds of translation[10–13]. Notably, RRF on its own is able to displace H69 from the subunit interface (**Fig. 3** and **Supplementary Fig. 1**), which is likely to be a necessary[31] but not sufficient step in the recycling process. EF-G binding to the ribosome–RRF complex, followed by GTP hydrolysis, would then complete the process of subunit dissociation. The present structural results showing that aminoglycosides bind to and stabilize H69 at the subunit interface, even in the presence of RRF, suggest how aminoglycosides inhibit ribosome recycling. The present structures also predict that destabilization of bridges between H69 in the large subunit and h44 in the small subunit might lead to some degree of aminoglycoside resistance, because increased dynamics in H69 would weaken binding of the aminoglycoside in its major groove (**Figs. 3** and **4**, **Supplementary Data** and **Supplementary Fig. 1**). Previously characterized mutations in H69 often lead to inactive ribosomes[32] and dominant lethality[31] (M. O'Connor, personal communication), which may preclude direct selection for aminoglycoside-resistance mutations in H69. However, single-site mutations conferring resistance to aminoglycosides arise in h44 of the 30S ribosomal subunit at nucleotides that, in addition to being involved in aminoglycoside binding to h44, also contribute to, or are located very close to, the intersubunit bridges with H69 in the 50S subunit[1,33]. It will therefore be interesting to test whether mutations in h44 have dual effects in reducing aminoglycoside binding to h44 as well as destabilizing bridges to H69.

In the present structures, RRF peels H69 away from the subunit interface upon binding to the 70S ribosome. This finding is seemingly at odds with the structure of the isolated *Deinococcus radiodurans* 50S ribosomal subunit in complex with domain I of RRF, where H69 is shifted away from the 50S body[30]—that is, toward where the subunit interface would be. One possibility is that the observed structural differences might reflect the conformations of the ribosome before and after RRF-induced subunit dissociation. In the intact ribosome, RRF destabilizes the subunit interface by breaking the intersubunit bridges made by H69. In the post-dissociation conformation of the 50S subunit, RRF may alter the conformation of H69 to prevent reassociation of the 50S subunit with the 30S subunit when RRF is present.

In addition to its effects on recycling, aminoglycoside binding to H69 may play a role in blocking mRNA and tRNA translocation. Both translocation and ribosome recycling are thought to involve a ratchet-like motion of the 30S subunit relative to the 50S subunit that rearranges bridges between H69 and the 30S subunit[26–28,34,35]. Biochemical data[36] support the idea that aminoglycoside binding to H69

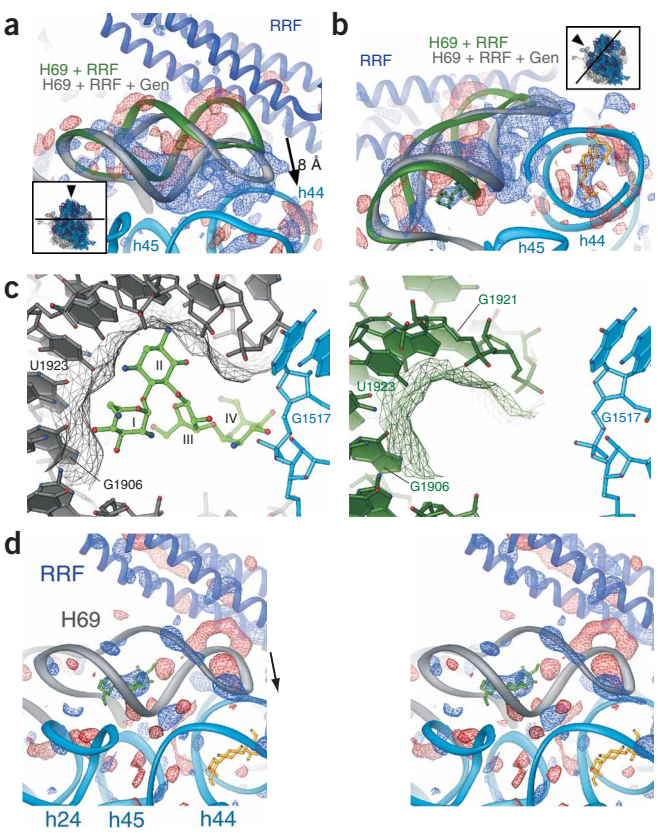

Figure 4 Structural effect of RRF on H69 is inhibited by aminoglycosides. (**a**) $F_o - F_o$ difference Fourier electron density map, at 4.2-Å resolution, of 70S ribosome I with RRF and gentamicin (Gen) bound, compared with 70S ribosome I containing RRF alone (**Supplementary Methods** and **Supplementary Data**). Coloring is as in **Figure 3**. Arrow shows direction of the conformational change in H69 upon gentamicin binding. (**b**) $F_o - F_o$ difference electron density map as in **a**. Gold and green, gentamicins bound to h44 and H69, respectively. (**c**) Changes in H69 major groove width in aminoglycoside-bound (left, RNA molecular surface in gray) and RRF-induced (right, RNA molecular surface in green) conformations. (**d**) Stereo view of the $F_o - F_o$ difference Fourier electron density map, truncated at 6-Å resolution, of 70S ribosome II in complex with RRF and with gentamicin at either saturating or low concentration (gentamicin data set 1; see **Table 1**, **Supplementary Methods** and **Supplementary Data**). The h44 binding site is fully occupied by antibiotic (gold) at both concentrations, yielding no difference density. When gentamicin binds to H69 with higher stoichiometry (positive density overlapping green antibiotic), there is a greater proportion of H69 at the interface (gray). Arrow indicates direction of the conformational change in H69 in the presence of saturating gentamicin, compared with the conformation of H69 at low gentamicin concentration.

may favor the ratcheted conformation of the ribosome[34]. Gentamicin, neomycin and paromomycin have been found to stabilize EF-G on the 70S ribosome in the presence of a non-hydrolyzable GTP analog, whereas the aminoglycoside hygromycin B, which binds only to h44 in the 70S ribosome (M.A.B., unpublished data), shows no effect[36]. Notably, neomycin inhibition of EF-G dissociation involves conversion of one ribosome population with a fast EF-G dissociation rate into a second population with a slow EF-G dissociation rate[36]. Cryo-EM reconstructions of the ribosome in the presence of EF-G and a non-hydrolyzable GTP analog have revealed that the ribosome adopts the ratcheted conformation in this complex[26,28], providing a structural explanation for these biochemical results.

In the recent structure of the *T. thermophilus* 70S ribosome with mRNA and tRNAs bound[20], paromomycin was found to bind only to the mRNA-decoding site on the 30S subunit, despite 100% conservation of the H69 binding site between *E. coli* and *T. thermophilus*[24]. By contrast, paromomycin binds to both the h44 and H69 sites in these crystals of the *E. coli* 70S ribosome (**Supplementary Figs. 2** and **3**). Notably, the conformations of H69 in the *T. thermophilus*[20] and the aminoglycoside-bound *E. coli* ribosome structures are identical within the coordinate error (r.m.s. deviation of ~0.7 Å for RNA residues surrounding the aminoglycoside-binding site). Furthermore, the accessibility of the H69 major groove in the structures is essentially identical (data not shown). The fact that aminoglycosides bind to H69 in the ribosome structures presented here is consistent with a prominent role for the H69 binding site in inhibiting ribosome recycling, when the A site is empty[10–13]. In contrast, paromomycin did not bind to H69 in the 70S ribosomal complex with A- and P-site tRNAs bound in the classical pre-translocation state (A/A and P/P tRNAs, with respect to the binding sites in the 30S/50S subunits)[20]; this supports the model in which 2-deoxystreptamine aminoglycosides bind to H69 preferentially when the ribosome adopts the ratcheted state, as noted above. It is also possible that the properties of ribosome crystals, which are grown in conditions far from the kinetically relevant ones, dampen ribosome fluctuations required for aminoglycoside binding to H69. Future biochemical and structural experiments will be needed to test for aminoglycoside binding to H69 in the ratcheted state.

The present structures reveal that widely used aminoglycosides of the 2-deoxystreptamine family bind to two sites in the ribosome, each of which contributes to inhibition of translation. The effect of aminoglycoside binding to H69 is to restrict H69 helical dynamics and thereby stabilize bridges between the ribosomal subunits. Whereas aminoglycoside binding to h44 in the 30S subunit is crucial for causing errors in mRNA decoding and may impede translocation, binding at the second site, in H69 of the 50S subunit, is likely to be important in inhibiting ribosome recycling and may lead to more potent inhibition of translocation. Translation inhibition by aminoglycoside binding to H69 of the large ribosomal subunit has implications for the design of new antibiotics and for improving existing aminoglycoside antibiotic therapy[2,37].

METHODS

Crystallization and data collection. Ribosomes from *E. coli* strain MRE600 depleted of protein S1 were crystallized as described[21]. Crystals were cryoprotected with buffers containing 20% (v/v) 2-methyl-2,4-pentanediol (MPD), 3% (w/v) PEG 8,000, 24.1% (v/v) PEG 400, 35 mM $MgCl_2$, 350 mM NH_4Cl, 1 mM spermine, 0.5 mM spermidine and 60 mM HEPES (pH 7.0) before flash-freezing in liquid nitrogen. Antibiotics at saturating concentrations[5,6,22] were soaked into crystals for 24 h during cryostabilization (0.005–0.01 mM of neomycin (a mixture of neomycin B and C; Sigma) or 0.4 mM of gentamicin C (a mixture of gentamicin C1a, C1 and C2; Fluka)). For experiments with RRF, *T. thermophilus* RRF, which functions with *E. coli* ribosomes[29], was purified as described[29], and 0.01 mM of the protein was soaked into crystals for 3 d during cryostabilization. For experiments with antibiotics and RRF, 0.4 mM or 0.005 mM of gentamicin, or 0.005 mM of paromomycin (Sigma), was soaked into crystals for 24 h, and then 0.01 mM of *T. thermophilus* RRF was soaked in along with the same concentration of the antibiotic for an additional 2 d, during cryostabilization. Throughout the text, references to the structure of 70S ribosome with RRF and gentamicin bound correspond to the one with a saturating concentration of gentamicin (0.4 mM) unless stated otherwise.

Diffraction data were measured using 1.11-Å-wavelength X-rays. Data for each complex were measured from either one or multiple crystals (**Table 1**) cooled to 93 K using 0.1°–0.3° oscillations at the SIBYLS (12.3.1) beamline at the Advanced Light Source, or at beamline 24-IDC at the Advanced Photon Source, each of which is equipped with an ADSC Q315 area detector. A modified strategy algorithm was used to optimize data measurement from multiple crystals. Data were reduced and scaled using DENZO/SCALEPACK[38] and TRUNCATE[39] (**Table 1**). The crystals diffract X-rays anisotropically, as indicated by the completeness of the data sets and signal-to-noise levels as a function of resolution (**Supplementary Fig. 4** online).

Structure refinement. The 3.5-Å structure of the *E. coli* 70S ribosome (PDB 2AVY, 2AW4, 2AW7 and 2AWB)[21] was used as the starting model for further refinement in CNS[40]. Initial models of gentamicin[41] and neomycin[19] were manually docked into $F_o - F_o$ difference electron density maps, made with the apo–70S ribosome as the reference and phases derived from Pirate density modification[42]. Topology and parameter files describing each antibiotic were generated with HIC-Up[43]. For the gentamicin C mixture, a model of gentamicin C1a was used for docking, as it has the highest affinity for the 30S ribosomal subunit among gentamicins C1a, C1 and C2 (ref. 41). Models were then refined using rounds of manual rebuilding with O[44] and torsional dynamics[40]. The refinement statistics are presented in **Table 1**. After torsional dynamics refinement, electron density maps were generated using sharpened $3F_o - 2F_c$ coefficients[40] and Pirate-derived phases.

The 2.6-Å structure of *T. thermophilus* RRF (PDB 1EH1)[45] was used as the starting model for RRF bound to the ribosome. To overcome non-isomorphism in $F_o - F_o$ difference electron density maps, diffraction data from crystals containing 70S ribosomes in complex with RRF were compared with diffraction data from crystals of the 70S ribosome in complex with neomycin, as a reference (**Supplementary Methods** online). The RRF model was first manually docked into the above $F_o - F_o$ difference electron density maps. Structure factor phases were derived from Pirate density modification. The complete model was then subjected to rigid-body refinement against diffraction data measured from crystals of the 70S ribosome in complex with RRF. The resulting models were further refined using rounds of manual rebuilding with O and torsional dynamics[40].

The interpretation of $F_o - F_o$ difference maps (such as those in **Fig. 4b** and **Supplementary Figs. 2** and **3**) initially relied on superpositions of the corresponding data with the high-resolution structural models of the 70S ribosome in complex with gentamicin, neomycin or RRF alone (**Table 1**). In the 70S ribosome structures with RRF and aminoglycosides bound, the difference density in the H69 region could be accounted for by rigid-body placement of the appropriate high-resolution structures. Subsequent torsional refinement of the structures of the ribosome in complexes with RRF and gentamicin and with RRF and paromomycin did not shift the positions of the antibiotics or H69 appreciably from their positions modeled by rigid-body docking into the $F_o - F_o$ difference density.

Figure preparation. The figures were made using Ribbons[46], ISIS Draw (MDL Information Systems), Origin (OriginLab) and Adobe Photoshop.

Accession codes. The coordinates and structure factors have been deposited in the Protein Data Bank with accession codes 2QB9, 2QBA, 2QBB, 2QBC (70S ribosome in complex with gentamicin), 2QAL, 2QAM, 2QAN, 2QAO (70S ribosome in complex with neomycin), 2QBD, 2QBE, 2QBF, 2QBG (70S ribosome in complex with RRF), 2QBH, 2QBI, 2QBJ, 2QBK (70S ribosome

Table 1 Diffraction statistics for *E. coli* 70S ribosome crystals in complex with aminoglycosides and/or RRF

	Gentamicin	Neomycin	RRF	RRF + gen (0.4 mM)	RRF + paro (data set 1)	RRF + paro (data set 2)[a]	RRF + gen (0.005 mM, data set 1)[a]	RRF + gen (0.005 mM, data set 2)[a]
Data collection								
Space group	$P2_12_12_1$	$P2_12_12_1$	$P2_12_12_1$	$P2_12_12_1$	$P2_12_12_1$	$P2_12_12_1$	$P2_12_12_1$	$P2_12_12_1$
Cell dimensions								
a, *b*, *c* (Å)	208.9, 379.2, 739.3	208.9, 379.2, 739.3	207.9, 378.2, 736.3	208.5, 378.9, 736.9	208.9, 378.8, 738.3	208.9, 379.2, 739.3	208.9, 379.2, 739.3	208.9, 379.2, 739.3
Resolution (Å)[b]	139–3.54 [3.81–3.54]	139–3.21 [3.7–3.21] (139–3.7)	123–3.3 [3.55–3.3] (123–3.55)	139–4.0 [4.4–4.0] (139–4.4)	69–4.45 [4.53–4.45]	69–4.53 [4.61–4.53]	69–4.4 [4.48–4.4]	69–4.2 [4.27–4.2]
R_{sym} or R^b_{merge}	10.2 [47.0]	11.2 [42.9]	10.4 [35.3]	8.3 [28.7]	9.6 [49.9]	12.5 [49.7]	7.4 [41.6]	13.1 [60.4]
$I / \sigma I$ [b]	10.6 [2.0]	8.8 [1.8]	12.5 [2.3]	12.1 [2.2]	11.7 [2.0]	10.5 [2.0]	10.1 [2.1]	9.4 [2.1]
Completeness (%)[b]	90.2 [54.8]	66.7 [12.1] (95.8)	88.0 [52.6] (96.8)	79.2 [32.6] (94.5)	95.6 [91.9]	88.1 [71.8]	93.5 [88.5]	97.9 [98.0]
Redundancy[b]	4.8 [1.6]	4.3 [1.3]	4.6 [1.6]	3.2 [1.5]	3.5 [2.4]	4.1 [1.9]	2.2 [1.6]	3.4 [3.0]
Refinement								
Resolution (Å)	70–3.54	70–3.21	40–3.3	40–4.15	40–4.45			
No. reflections	627,816	626,435	738,488	382,478	341,210			
R_{work} / R_{free}	27.8 / 31.6	27.4 / 30.9	27.5 / 30.4	26.1 / 30.4	26.3 / 30.9			
No. atoms	284,290	284,210	286,998	287,122	287,166			
Mean *B*-factor	74.9	75.5	69.7	76.5	76.3			
R.m.s. deviations								
Bond lengths (Å)	0.003	0.003	0.003	0.003	0.003			
Bond angles (°)	0.923	0.905	0.928	0.953	0.940			

For the structure of 70S ribosome in complex with gentamicin, 19 crystals were used for data measurement; for the complex with neomycin, 10 crystals were used; for the complex with RRF, 14 crystals were used; for the complexes with RRF and gentamicin (gen), one crystal was used in each case; for the complexes with RRF and paromomycin (paro), two crystals were used in each case. [a]Data from crystals with paromomycin bound (data set 2) and two crystals with gentamicin bound at low concentration (0.005 mM, data sets 1 and 2) were used only for calculations of the difference maps (**Fig. 4d** and **Supplementary Figs. 2** and **3**), to overcome non-isomorphism between crystals. [b]Values in parentheses are for the resolution range with a high level of data completion (**Supplementary Fig. 4**). Values in square brackets are for the highest-resolution shell. Owing to anisotropic diffraction, the highest-resolution shell often has low levels of completion (**Supplementary Fig. 4**).

in complex with RRF and gentamicin) and 2Z4K, 2Z4L, 2Z4M, 2Z4N (70S ribosome in complex with RRF and paromomycin).

Note: Supplementary information is available on the Nature Structural & Molecular Biology website.

ACKNOWLEDGMENTS

We thank K. Frankel, S. Classen and G. Meigs for help with data measurement at the SIBYLS and 8.3.1 beamlines at the Advanced Light Source; K. Rajashankar, I. Kourinov and N. Sukumar for help with data measurement at Northeastern Collaborative Access Team beamline 24-IDC at the Advanced Photon Source; W. Wintermeyer, M. O'Connor and K. Fredrick for helpful discussions; A. Borovinskiy for help with figure preparation and overall support; and J. Doudna, H. Noller, P. Gunda and J. Dunkle for helpful comments on the manuscript. This work was supported by US National Institutes of Health (NIH) grants GM65050 (J.H.D.C.) and GM60429 (A.K.), the Nippon Paint Fund (H.K.), NIH National Cancer Institute grant CA92584 (for the SIBYLS and 8.3.1 beamlines), NIH National Center for Research Resources grant RR-15301 (for beamline 24-IDC) and US Department of Energy grants DE-AC03-76SF00098, KP110201, and LBNL LDRD 366851 (J.H.D.C.), DE-AC03 76SF00098 (for the SIBYLS and 8.3.1 beamlines) and DE-AC02-06CH11357 (for the Advanced Photon Source).

COMPETING INTERESTS STATEMENT

The authors declare no competing financial interests.

Published online at http://www.nature.com/nsmb/
Reprints and permissions information is available online at http://npg.nature.com/reprintsandpermissions

1. Magnet, S. & Blanchard, J.S. Molecular insights into aminoglycoside action and resistance. *Chem. Rev.* **105**, 477–498 (2005).
2. Sutcliffe, J.A. Improving on nature: antibiotics that target the ribosome. *Curr. Opin. Microbiol.* **8**, 534–542 (2005).
3. Davies, J., Gorini, L. & Davies, B.D. Misreading of RNA codewords induced by aminoglycoside antibiotics. *Mol. Pharmacol.* **1**, 93–106 (1965).
4. Davies, J., Jones, D.S. & Khorana, H.G. A further study of misreading of codons induced by streptomycin and neomycin using ribopolynucleotides containing two nucleotides in alternating sequence as templates. *J. Mol. Biol.* **18**, 48–57 (1966).
5. Cabañas, M.J., Vázquez, D. & Modolell, J. Inhibition of ribosomal translocation by aminoglycoside antibiotics. *Biochem. Biophys. Res. Commun.* **83**, 991–997 (1978).
6. Misumi, M., Nishimura, T., Komai, T. & Tanaka, N. Interaction of kanamycin and related antibiotics with the large subunit of ribosomes and the inhibition of translocation. *Biochem. Biophys. Res. Commun.* **84**, 358–365 (1978).
7. Hirokawa, G. *et al.* Post-termination complex disassembly by ribosome recycling factor, a functional tRNA mimic. *EMBO J.* **21**, 2272–2281 (2002).
8. Wilson, D.N. & Nierhaus, K.H. The how and Y of cold shock. *Nat. Struct. Mol. Biol.* **11**, 1026–1028 (2004).
9. Janosi, L. *et al.* Evidence for *in vivo* ribosome recycling, the fourth step in protein biosynthesis. *EMBO J.* **17**, 1141–1151 (1998).
10. Zavialov, A.V., Hauryliuk, V.V. & Ehrenberg, M. Splitting of the posttermination ribosome into subunits by the concerted action of RRF and EF-G. *Mol. Cell* **18**, 675–686 (2005).
11. Gao, N. *et al.* Mechanism for the disassembly of the posttermination complex inferred from cryo-EM studies. *Mol. Cell* **18**, 663–674 (2005).
12. Peske, F., Rodnina, M.V. & Wintermeyer, W. Sequence of steps in ribosome recycling as defined by kinetic analysis. *Mol. Cell* **18**, 403–412 (2005).
13. Hirokawa, G., Demeshkina, N., Iwakura, N., Kaji, H. & Kaji, A. The ribosome-recycling step: consensus or controversy? *Trends Biochem. Sci.* **31**, 143–149 (2006).
14. Hirokawa, G. *et al.* The role of ribosome recycling factor in dissociation of 70S ribosomes into subunits. *RNA* **11**, 1317–1328 (2005).
15. Teyssier, E. *et al.* Temperature-sensitive mutation in yeast mitochondrial ribosome-recycling factor (RRF). *Nucleic Acids Res.* **31**, 4218–4226 (2003).
16. Rolland, N. *et al.* Plant ribosome recycling factor homologue is a chloroplastic protein and is bactericidal in *Escherichia coli* carrying temperature-sensitive ribosome recycling factor. *Proc. Natl. Acad. Sci. USA* **96**, 5464–5469 (1999).
17. Janosi, L., Shimizu, I. & Kaji, A. Ribosome recycling factor (ribosome releasing factor) is essential for bacterial growth. *Proc. Natl. Acad. Sci. USA* **91**, 4249–4253 (1994).

18. Campuzano, S., Vázquez, D. & Modolell, J. Functional interaction of neomycin B and related antibiotics with 30S and 50S ribosomal subunits. *Biochem. Biophys. Res. Commun.* **87**, 960–966 (1979).
19. Carter, A.P. *et al.* Functional insights from the structure of the 30S ribosomal subunit and its interactions with antibiotics. *Nature* **407**, 340–348 (2000).
20. Selmer, M. *et al.* Structure of the 70S ribosome complexed with mRNA and tRNA. *Science* **313**, 1935–1942 (2006).
21. Schuwirth, B.S. *et al.* Structures of the bacterial ribosome at 3.5 Å resolution. *Science* **310**, 827–834 (2005).
22. Moazed, D. & Noller, H.F. Interaction of antibiotics with functional sites in 16S ribosomal RNA. *Nature* **327**, 389–394 (1987).
23. Yusupov, M.M. *et al.* Crystal structure of the ribosome at 5.5 Å resolution. *Science* **292**, 883–896 (2001).
24. Cannone, J.J. *et al.* The comparative RNA web (CRW) site: an online database of comparative sequence and structure information for ribosomal, intron, and other RNAs. *BMC Bioinformatics* **3**, 2 (2002).
25. Lancaster, L., Kiel, M.C., Kaji, A. & Noller, H.F. Orientation of ribosome recycling factor in the ribosome from directed hydroxyl radical probing. *Cell* **111**, 129–140 (2002).
26. Valle, M. *et al.* Locking and unlocking of ribosomal motions. *Cell* **114**, 123–134 (2003).
27. Agrawal, R.K. *et al.* Visualization of ribosome-recycling factor on the *Escherichia coli* 70S ribosome: functional implications. *Proc. Natl. Acad. Sci. USA* **101**, 8900–8905 (2004).
28. Connell, S.R. *et al.* Structural basis for interaction of the ribosome with the switch regions of GTP-bound elongation factors. *Mol. Cell* **25**, 751–764 (2007).
29. Raj, V.S., Kaji, H. & Kaji, A. Interaction of RRF and EF-G from *E. coli* and *T. thermophilus* with ribosomes from both origins—insight into the mechanism of the ribosome recycling step. *RNA* **11**, 275–284 (2005).
30. Wilson, D.N. *et al.* X-ray crystallography study on ribosome recycling: the mechanism of binding and action of RRF on the 50S ribosomal subunit. *EMBO J.* **24**, 251–260 (2005).
31. Ali, I.K., Lancaster, L., Feinberg, J., Joseph, S. & Noller, H.F. Deletion of a conserved, central ribosomal intersubunit RNA bridge. *Mol. Cell* **23**, 865–874 (2006).
32. Liiv, A., Karitkina, D., Maiväli, U. & Remme, J. Analysis of the function of *E. coli* 23S rRNA helix-loop 69 by mutagenesis. *BMC Mol. Biol.* **6**, 18 (2005).
33. Rackham, O., Wang, K. & Chin, J.W. Functional epitopes at the ribosome subunit interface. *Nat. Chem. Biol.* **2**, 254–258 (2006).
34. Frank, J. & Agrawal, R.K. A ratchet-like intersubunit reorganization of the ribosome during translocation. *Nature* **406**, 318–322 (2000).
35. Horan, L.H. & Noller, H.F. Intersubunit movement is required for ribosomal translocation. *Proc. Natl. Acad. Sci. USA* **104**, 4881–4885 (2007).
36. Campuzano, S., Vázquez, D. & Modolell, J. Dissociation of guanosine nucleotide-elongation factor G-ribosome complexes. *Biochemistry* **18**, 1570–1574 (1979).
37. Senior, K. Duchenne muscular dystrophy improved by gentamicin. *Mol. Med. Today* **5**, 461 (1999).
38. Otwinowski, Z. & Minor, W. Processing of X-ray diffraction data collected in oscillation mode. *Methods Enzymol.* **276**, 307–326 (1997).
39. Collaborative Computational Project, Number 4. The CCP4 suite: programs for protein crystallography. *Acta Crystallogr. D Biol. Crystallogr.* **50**, 760–763 (1994).
40. Brünger, A.T. *et al.* Crystallography & NMR system: a new software suite for macromolecular structure determination. *Acta Crystallogr. D Biol. Crystallogr.* **54**, 905–921 (1998).
41. Yoshizawa, S., Fourmy, D. & Puglisi, J.D. Structural origins of gentamicin antibiotic action. *EMBO J.* **17**, 6437–6448 (1998).
42. Cowtan, K. General quadratic functions in real and reciprocal space and their application to likelihood phasing. *Acta Crystallogr. D Biol. Crystallogr.* **56**, 1612–1621 (2000).
43. Kleywegt, G.J. & Jones, T.A. Databases in protein crystallography. *Acta Crystallogr. D Biol. Crystallogr.* **54**, 1119–1131 (1998).
44. Jones, T.A., Zou, J.Y., Cowan, S.W. & Kjeldgaard, M. Improved methods for building protein models in electron density maps and the location of errors in these models. *Acta Crystallogr. A* **47**, 110–119 (1991).
45. Toyoda, T. *et al.* Crystal structure combined with genetic analysis of the *Thermus thermophilus* ribosome recycling factor shows that a flexible hinge may act as a functional switch. *RNA* **6**, 1432–1444 (2000).
46. Carson, M. Ribbons. *Methods Enzymol.* **277**, 493–502 (1997).